Carbohydrate Polymers 92 (2013) 1116–1123

Contents lists available at SciVerse ScienceDirect

Carbohydrate Polymers

journal homepage: www.elsevier.com/locate/carbpol

Bionanowhiskers from jute: Preparation and characterization

Nibedita Kasyapi, Vidhi Chaudhary, Anil K. Bhowmick*

Department of Materials Science and Engineering, School of Engineering and Technology, Indian Institute of Technology Patna, Patna 800013, India

ARTICLE INFO

Article history:
Received 14 May 2012
Received in revised form 31 August 2012
Accepted 9 October 2012
Available online 17 October 2012

Keywords:
Jute
Nanowhisker
Nanoparticle
Acid hydrolysis
Hemicellulose

ABSTRACT

Bionanowhiskers were extracted from jute by acid hydrolysis. At first cellulose microfibrils were formed by alkali treatment. Addition of an acid to the microfibrils triggered the formation of cellulose nanowhiskers. These were characterized by using different techniques *viz.* Fourier transform infrared spectroscopy (FTIR), X-ray diffraction (XRD), thermogravimetry (TGA), scanning electron microscopy (SEM) and atomic force microscopy (AFM). In the FTIR study, absence of peak at 1738 cm^{-1} indicated removal of hemicellulose. The rod like morphology of the nanowhiskers (length – 550 ± 100 nm, width – 77 ± 30 nm) was observed after 1 h of acid hydrolysis, whereas further increase in time resulted in triangular shape morphology. Acid hydrolysis increased crystallinity, but decreased the temperature corresponding to major degradation (T_{max}) and onset of degradation (T_i). These bionanowhiskers might be useful as reinforcing element in nanocomposites.

© 2012 Elsevier Ltd. All rights reserved.

1. Introduction

Cellulose, the most abundant biomass material, can replace the synthetic polymer and is gaining importance as a green and sustainable material in recent years because of paucity of fossil fuel. It can be easily derived from plants, woods, grasses and algae. The cellulosic fiber can be easily extracted from cotton, kapok, flax, hemp, jute, ramie, sisal, and coir (Kahil, Bhat, Ireana, & Yusra, 2011; Siqueira, Bras, & Dufresne, 2010). Cellulose, with unique structural features, has found huge application from paper industry to fascinating world of nanotechnology (Favier, Chanzy, & Cavaille, 1995). In the field of nanocomposites, cellulose has been used as reinforcing phase in the form of microfibrils, microcrystals, nanocrystals and nanowhiskers (Beck-Candanedo, Roman, & Gray, 2005). These nanostructures are differentiated based on their size, shape, and length to diameter ratio.

Cellulose consists of linear polysaccharides of unbranched β (1,4) linked glucopyranose units (Kahil et al., 2011). Cellulose obtained from the plant mainly constitutes crystallites with interdispersed amorphous regions in it. This cellulose is called native cellulose or cellulose I, showing parallel arrangement of glucan-chains. Another polymorph which is commonly used to designate the cellulose precipitated out of solution, is regenerated cellulose called cellulose II, having antiparallel arrangement of glucanchains. Cellulose II is thermodynamically more stable than cellulose I (Siqueira et al., 2010). Further investigation shows that the native cellulose contains two crystalline allomorphs, *i.e.* cellulose I_α and cellulose I_β. Cellulose I_α has triclinic cell arrangement, mostly found in algae and bacterial cellulose whereas cellulose I_β is monoclinic allomorph, present in ramie and cotton (Siqueira et al., 2010). The ratio of these two allomorphs varies from plant to plant.

Now-a-days, the most well-liked application of cellulose is in biobased nanocomposite materials, in which cellulose is mostly used as reinforcing agent. In some cases, it is also used as matrix material as reported by Pullawan, Wilkinson, and Eichhorn (2010). The other preferred matrix materials are polycaprolactone (PCL) (Siqueira, Bras, & Dufresne, 2009), polylactic acid (PLA) (Goffin et al., 2011; Oksman, Etang, Mathew, & Jonoobi, 2011) and polyhydroxybutyrate (PHA) (Kahil et al., 2011). The disadvantages of cellulose are high moisture absorptivity, low thermal stability, difficulty in processing and poor compatibility with polymer matrices (for which grafting is used).

Cellulose, used in reinforcement, may be in different forms among which whiskers are very popular. Cellulose nanowhiskers are rod like nanoparticles having width less than 100 nm. These are basically crystals of cellulose in nanorange. These nanowhiskers are synthesized by acid hydrolysis as reported by many authors in order to disrupt the amorphous domains of cellulose through penetration of hydronium ions promoting the cleavage of glycosidic bonds releasing cellulose crystallites (Siqueira et al., 2010). The hydrolysis time, temperature, choice of suitable acid, acid concentration and acid to cellulose ratio have great effect on the size, morphology and chemical structure of the developed whiskers. Several natural resources have been used to prepare cellulose whiskers like ramie (Goffin et al., 2011), coconut husk (Rosa et al., 2010), bioresidue from wood during bioethanol production (Oksman et al., 2011), cotton (Capadona et al., 2009; Satyamurthy, Jain, Balasubramanya, & Vigneshwaran, 2011), algae (Sugiyama, Chanzi, & Revol, 1994),

* Corresponding author. Tel.: +91 612 2552001; fax: +91 612 2277384.
E-mail addresses: anilkb@rtc.iitkgp.ernet.in, director@iitp.ac.in (A.K. Bhowmick).

0144-8617/$ – see front matter © 2012 Elsevier Ltd. All rights reserved.
http://dx.doi.org/10.1016/j.carbpol.2012.10.021

Table 1
Sample information of Bio-nanowhishkers.

Sample code	Sample composition	Reagent used	Reaction temperature	Reaction time
NJ	Regenerated cellulose or pulp	2% NaOH	60 °C	48 h
BJ	Bleached pulp	30% H_2O_2	Room temperature	12 h
J0.51	Bleached pulp	27.7% H_2SO_4	45 °C	30 min
J11	Bleached pulp	27.7% H_2SO_4	45 °C	1 h
J21	Bleached pulp	27.7% H_2SO_4	45 °C	2 h
J41	Bleached pulp	27.7% H_2SO_4	45 °C	4 h
J14	Bleached pulp	65% H_2SO_4	45 °C	1 h
J12	Bleached pulp	27.7% H_2SO_4	57 °C	1 h
J13	Bleached pulp	85% HCOOH	45 °C	1 h

hemp (Cao, Chen, Chang, Stumborg, & Huneault, 2008), tunicin (Bonini et al., 2002; Favier et al., 1995), sisal (Garcia de Rodriguez, Thielemans, & Dufresne, 2006), wood (Beck-Candanedo et al., 2005), sugerbeet (Azizi Samir, Alloin, Paillet, & Dufresne, 2004), bacteria (Marta, Amparo, & Jose, 2011), and rice husk (Rosa, Rehman, de Miranda, Nachtigall, & Bica, 2012). The shape and dimension of nanowhisker, to a certain extent also depend on the type of resource used.

Jute, low cost vegetable fiber having 60.7% cellulose content, is widely grown in the tropical countries like India and Bangladesh. Till date, no article has been reported on nanowhisker preparation using jute as raw material.

In this work, we have prepared cellulose nanowhiskers using jute, by acid hydrolysis at different times and temperatures, with varying acid concentration and using different acids. These whiskers have been characterized by FTIR, XRD, SEM, AFM and TGA. Their most likely application would be as a reinforcing agent in nanocomposites for energy storage devices replacing cellulose or carbon nanotube (Chen, Kim, Kwon, Yun, & Jin, 2009).

2. Experimental

2.1. Materials

Commercially available jute fibers of "tossa-daisee" (Corchorus olitorius) variety of TDS grade, as per IS: 271–2003, were used for this study. All other solvents and reagents were used as received from the commercial source.

2.2. Preparation of cellulose nanowhisker

Jute fibers were dried at 90 °C and cut into small size (1–2 cm). Then the fibers were dewaxed using toluene with mild heating. The dewaxed material was soaked in 2% NaOH solution for overnight followed by heating at around 60 °C. This process was continued for 2 days. This removed the non-cellulosic materials from the cellulose. This cellulose, called regenerated cellulose or pulp (NJ) which was repeatedly washed with distilled water to get rid of the alkali. The NJ was bleached with 30% H_2O_2 solution for overnight. The bleached pulp (BJ) was washed with abundant distilled water and dried. 0.5 gm of BJ was treated with 27 ml of 27.7% sulphuric acid (H_2SO_4) at 45 °C at different time intervals *viz.* 30 min (J0.51), 1 h (J11), 2 h (J21), 4 h (J41). After acid hydrolysis, the material was poured in ice cold water and filtered using nylon membrane. It was thoroughly rinsed with distilled water to neutralize the acid and dried at 60 °C for 5 h. In addition to the above time variation, the effect of acid hydrolysis was studied also by varying 3 other parameters: (i) nature of acid, (ii) acid concentration, and (iii) temperature. To investigate the effect of acid, BJ was treated with formic acid (HCOOH) for 1 h at 45 °C (J13). Two different concentrations of H_2SO_4 were used *viz.* 27.7% H_2SO_4 (J11) and 65% H_2SO_4 (J14). The acid hydrolysis was carried out at different temperatures to study effect of temperature *viz.* 45 °C (J11) and 57 °C (J12). The details of different samples are furnished in Table 1. The whiskers were characterized in each step of its preparation to observe the changes occurred in the material using various techniques.

2.3. Characterization

2.3.1. Fourier transform infrared spectroscopy (FTIR)

FTIR analysis was carried out to obtain molecular fingerprint of the sample. The analysis was done in universal attenuated total reflectance mode (UATR) using Perkin Elmer Spectrum 400 machine in a spectral range of 4000–530 cm^{-1} with a total of 16 scans per sample.

2.3.2. X-ray diffraction (XRD)

The diffraction profile was recorded for each sample in order to examine the change in crystallinity of the material using Rigaku TT RAX 3XRD machine in the range of 10–50° (2θ) with CuKα (1.54 Å) as radiation source and 50 kV voltage and 100 mA intensity.

2.3.3. Scanning electron microscopy (SEM)

The surface morphology of the samples was studied with the help of field emission scanning electron microscope (Hitachi, S-4800 FESEM) by applying accelerating voltage from 10 to 15 kV. Very little amount of sample, dispersed in acetone, was put on a conducting carbon tape stuck on the stub and coated with gold by using Hitachi E-1010 Ion Sputter system.

2.3.4. Atomic force microscopy (AFM)

The AFM measurements were performed on Agilent 5500 scanning probe microscope. AFM images were recorded in non-contact mode at room temperature. Commercial probes were used with a spring constant of 21–98 N/m and a resonance frequency of about 146–236 kHz. For AFM analysis of the cellulose nanowhiskers, a drop of the whisker suspension was allowed to dry on a mica surface.

2.3.5. Thermogravimetry (TG)

The thermogravimetric analysis was carried out on TA instruments SDT Q 600 system at a ramp rate of 10 °C/min under nitrogen atmosphere (flow rate – 100 ml/min) from the room temperature to 800 °C.

3. Results and discussion

3.1. FTIR analysis

The FTIR spectra of raw jute, BJ and J11 are shown in Fig. 1a and the corresponding data are summarized in Table 2. The samples BJ and J11 represent jute after bleaching and then acid treatment respectively. The subsequent sections will deal with the samples treated with acid at different times and temperatures. Nature of acid and acid concentration were also varied. In raw jute, the broad peak in the range of 3336 cm^{-1} appears due to O—H stretching

Table 2
Peak positions (cm^{-1}) of FTIR spectrum for samples.

Sample					Possible assignments
Raw jute	BJ	J11	J21	J41	
3336	3335	3336	3334	–	O—H stretching
2921, 2853	2901	2896	2895	2898	Aliphatic saturated C—H stretching vibration in cellulose and hemicellulose
1738	–	–	–	–	C=O stretching vibration of carboxylic acid and ester in hemicellulose
1646	–	–	–	–	Absorbed water
1594	1592	1593	1592	1589	Aromatic C=C vibration
1505					Lignin component (Rosa et al., 2012)
1456	–	–	–	–	Lignin component (Ray & Sarkar, 2001)
1424	1422	1423	1423	1423	Bending vibration for C_6—CH_2 due to deformation of wagging (Lu & Hsieh, 2010)
1316	1316	1316	1316	1316	Deformation vibration frequency for C—OH and CH groups
1242	–	–	–	–	C—O stretching of ether linkage for lignin (Rosa et al., 2012)
1158	1159	1160	1159	1159	Antisymmetric bridge C—O—C stretching (glycosidic ring)
1103	1105	1105	1105	1106	C—O/C—C stretching vibration for ring
1051	1051	1053	1053	1054	C—O/C—C stretching vibration (C_3—O_3)
1030	1029	1030	1029	1030	C—O/C—C stretching vibration (C_6—H_2—O_6)
896	897	895	895	895	β-Glucosidic linkage
666	–	662	663	662	Out of plane bending vibration of intermolecular H-bonded O—H group
		557	558	557	Torsional vibration of pyranose ring

vibrations, and the peaks at 2921 cm^{-1} and 2853 cm^{-1} arise due to C—H stretching vibrations in cellulose and hemicellulose. The sharp peak at 1738 cm^{-1} for C=O stretching gives evidence of carboxylic acid and ester group present in the hemicellulose, which entirely disappears in the treated samples. The peak at 898 cm^{-1} confirms the presence of β-gluocosidic linkage. The peak at 1030 cm^{-1} corresponds to C—O and C—C stretching vibrations (Ray & Sarkar, 2001). In comparison to raw jute, the peak area at 3336 cm^{-1} shows a decrease for BJ. For J11, similar decrease is observed. The peak at 2921 cm^{-1} shifts toward lower value indicating the removal of hemicelluloses, which is also supported by disappearance of the peak at 1738 cm^{-1}. The decrease in the intensity for the peaks at 1505 cm^{-1} and 1456 cm^{-1} after alkali treatment is a sign of partial removal of lignin (Ray & Sarkar, 2001; Rosa et al., 2012).

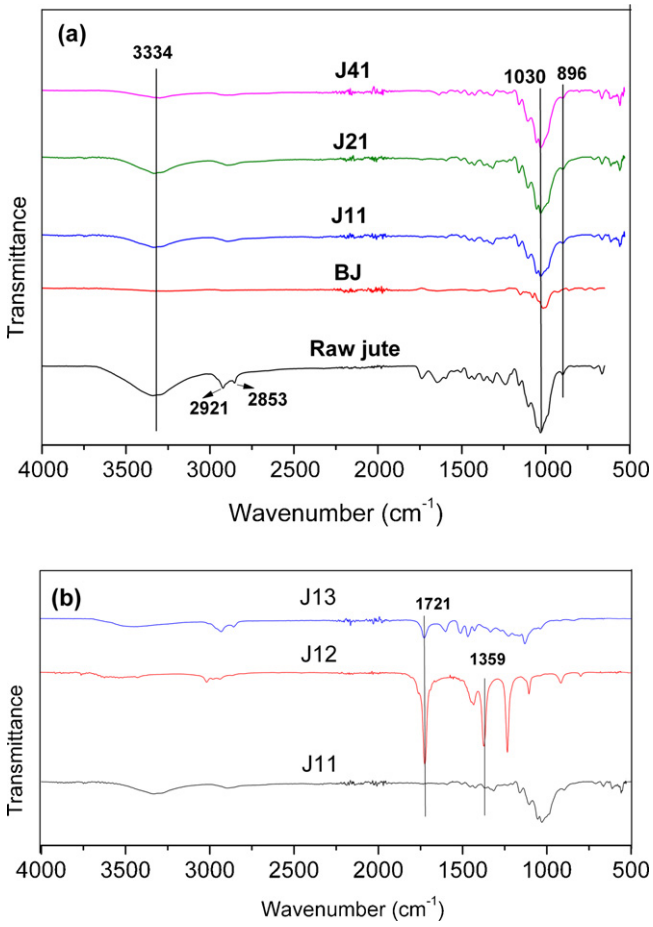

Fig. 1. FTIR spectra of (a) raw jute, BJ, J11, J21 and J41; (b) J11, J12 and J13.

3.2. XRD analysis

The X-ray diffraction pattern of the samples (raw jute, BJ and J11) is given in Fig. 2. In the raw jute, the major crystalline peak corresponding to cellulose appears at 22.4° (2θ) for 2 0 0 crystallographic plane (Lu & Hsieh, 2010; Rosa et al., 2012). The intensity of this peak increases on modification. A small hump at 16° is also noticed. The increase in the peak intensity, with a little shift of 2θ from 22.4° to 22.6° indicates improvement in the crystallinity as well as gives evidence for transformation of cellulose I_α into cellulose I_β after alkali treatment, as supported by literature (Wada, Heux, & Sugiyama, 2004). The small hump at 16° arises due to overlapping of 1 1 0 and 1 $\bar{1}$ 0 planes of cellulose I_β (Ouajai & Shanks, 2005). The crystallinity index for all samples was determined by using the following formula (Terinte, Ibbett, & Schuster, 2011):

$$\%\,\text{crystallinity} = 100 \times \frac{I_{200} - I_{\text{non-cr}}}{I_{200}} \quad (1)$$

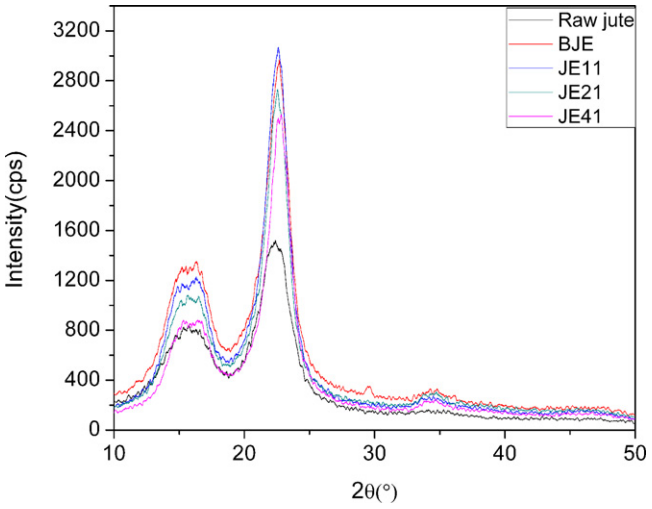

Fig. 2. XRD patterns of raw jute, BJ, J11, J21 and J41.

where I_{200} represents maximum intensity of the peak corresponding to the plane 200 and $I_{\text{non-cr}}$ is the intensity for diffraction of non-crystalline material, *i.e.* valley between the peaks.

For measuring the crystallite size of the samples, the following expression is used (Mondal & Bhowmick, 2012):

$$\text{Cs} = \frac{0.9\lambda}{\beta \cos\theta} \quad (2)$$

where Cs is the crystallite size, β is the full width at half maxima, λ is the wavelength of the X-ray, and θ is half of the angle for the corresponding peak (2θ).

The value of % crystallinity, crystallite size and 2θ for all samples is given in Table 3. The results exhibit that crystallinity increases upon treatment with alkali followed by bleaching (BJ), which further increases on acid hydrolysis (J11). The removal of amorphous region by acid treatment adds to the crystallinity. There is an

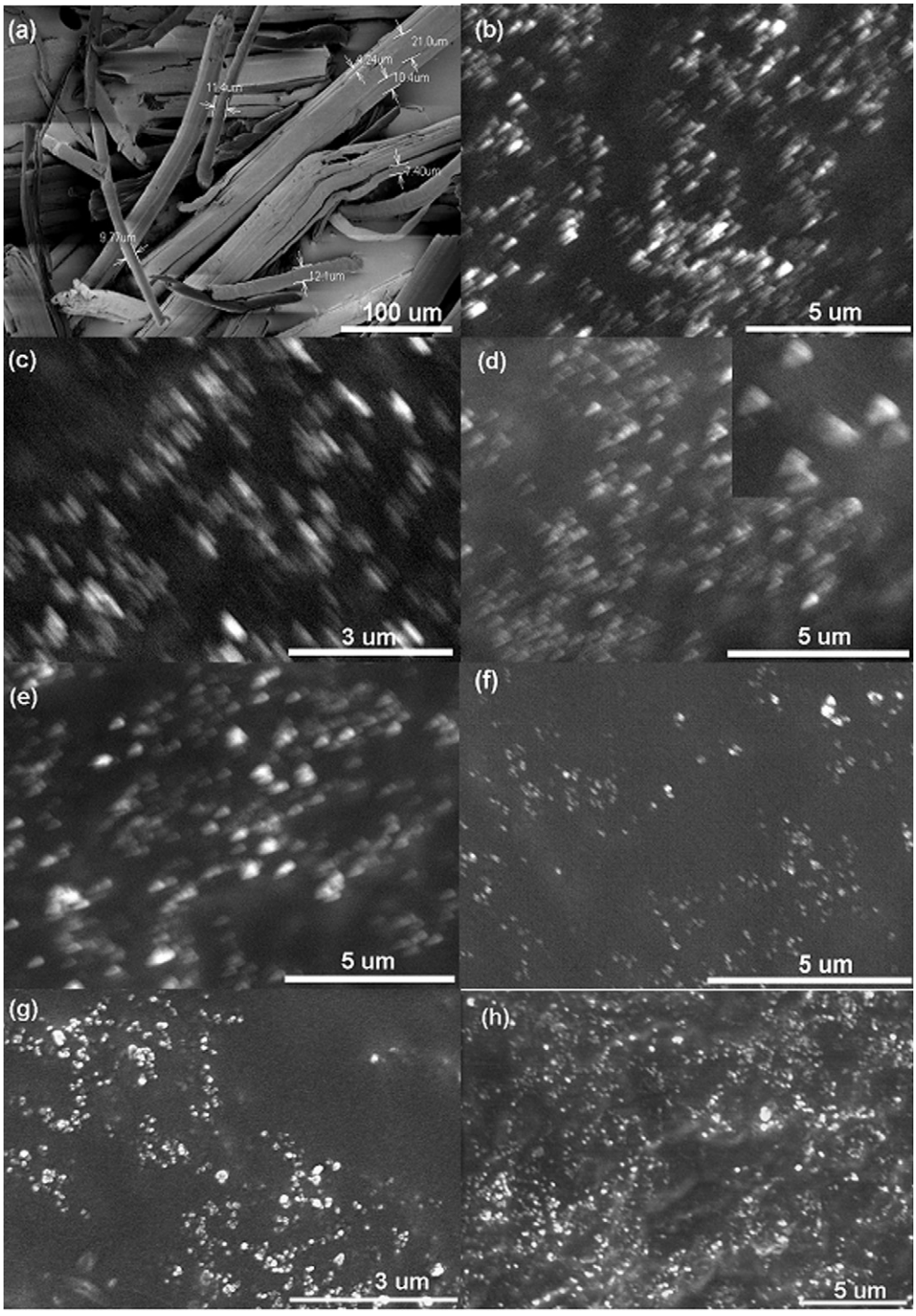

Fig. 3. FESEM images of (a) BJ; (b) J0.51; (c)J11; (d)J21; (e)J41; (f) J12; (g) J13 and (h) J14.

Table 3
Different parameters for samples from XRD patterns.

Sample	2θ (°)	% crystallinity	Crystallite size (nm)
Raw jute	22.4	77.0	2.8
BJ	22.9	82.0	3.7
J11	22.6	84.0	4.2
J21	22.6	84.0	4.1
J41	22.7	85.0	4.2

Table 4
Different thermal parameters for samples from TGA and DTG curves.

Sample	T_i (°C)	T_{max} (°C)	Residue (wt%)	DTG (wt%/min) at T_{max}
Raw jute	328.5	363.1	11.8	15.3
BJ	335.9	363.9	11.4	18.3
J11	278.8	334.1	14.5	9.0
J21	260.7	332.8	16.4	6.8
J41	262.0	330.6	10.2	7.5

enormous increase in the crystallite size in the case of BJ, which increases further on acid hydrolysis (J11) (Table 3). The crystallite size (4.2 nm) of nanowhiskers matches well with that (4.42 nm) obtained from rice straw (Lu & Hsieh, 2012). Thus, an increase in crystallinity favors the formation of cellulose nanowhiskers.

3.3. SEM analysis

To further prove the growth of nanowhiskers, FESEM images of the samples (BJ and J11) are taken and shown in Fig. 3. For BJ (Fig. 3a), the width of the fibers is in the micrometer range. After acid hydrolysis of BJ at different time intervals, cellulose whiskers are observed in J11 (Fig. 3c) exhibiting the uniform rod like structure with L/D ratio of 6.5 (length – 550 ± 100 nm, width – 77 ± 30 nm). The length (L) and width (D) of the whisker for J11 are greater than those obtained from sisal (Siqueira et al., 2009), cotton (Capadona et al., 2009; Satyamurthy et al., 2011), microcrystalline cellulose (Capadona et al., 2009; Kvien, Tanem, & Oksman, 2005) and rice husk (Rosa et al., 2012).

3.4. AFM analysis

AFM images of cellulose nanowhiskers (J11, J21) are exhibited in Fig. 4a and b. Several whiskers are agglomerated side-by-side. The shape of the whiskers appears, however, almost the same as that observed in FESEM for the same sample. The whiskers are measured to be 500–600 nm long, *i.e.* in the same range as that from FESEM. The width of the nanowhiskers is observed in the range of 25–50 nm. The dimension of the whiskers for J21 is also similar to that observed in FESEM.

3.5. TGA analysis

Fig. 5a and b show the thermograms depicting weight loss as function of temperature and DTG curves for all representative samples under nitrogen atmosphere. The temperature corresponding to maximum degradation (T_{max}), the onset of degradation (T_i), residue and maximum rate of degradation (Choudhury, Bhowmick, & Ong, 2010) for all samples are tabulated in Table 4. The TGA analysis reveals that there is a significant change in composition between raw jute and the cellulose derived from it. In the DTG curve (Fig. 5b) of raw jute, a small shoulder close to the degradation peak is observed, which occurs due to presence of impurities (lignin, hemicelluloses as supported by FTIR data) other than cellulose, but this shoulder is completely absent in the BJ, a sign of removal of noncellulosic materials. The degradation of raw jute starts at 328.5 °C, which is less than the onset degradation of temperature of BJ (Fig. 5a). This is because of removal of non-cellulosic materials and increase of crystallinity in BJ (Kaushik, Singh, & Verma, 2010). Interestingly, on acid hydrolysis the onset of degradation (T_i) is observed to be decreased, which may be attributed to the fact that the formation of cellulose nanocrystals leads to increase in surface area, therefore more exposure to the heat and heat transfer is facilitated (Lu & Hsieh, 2010). The major degradation temperature (T_{max}) remains same in raw jute and BJ, whereas it decreases by almost 30 °C after acid hydrolysis (J11); however XRD data shows increase in crystallinity after acid hydrolysis. It is clear from the data (Table 4) that residue left after complete degradation is always found to be more in sample J11 than in BJ and the rate of degradation

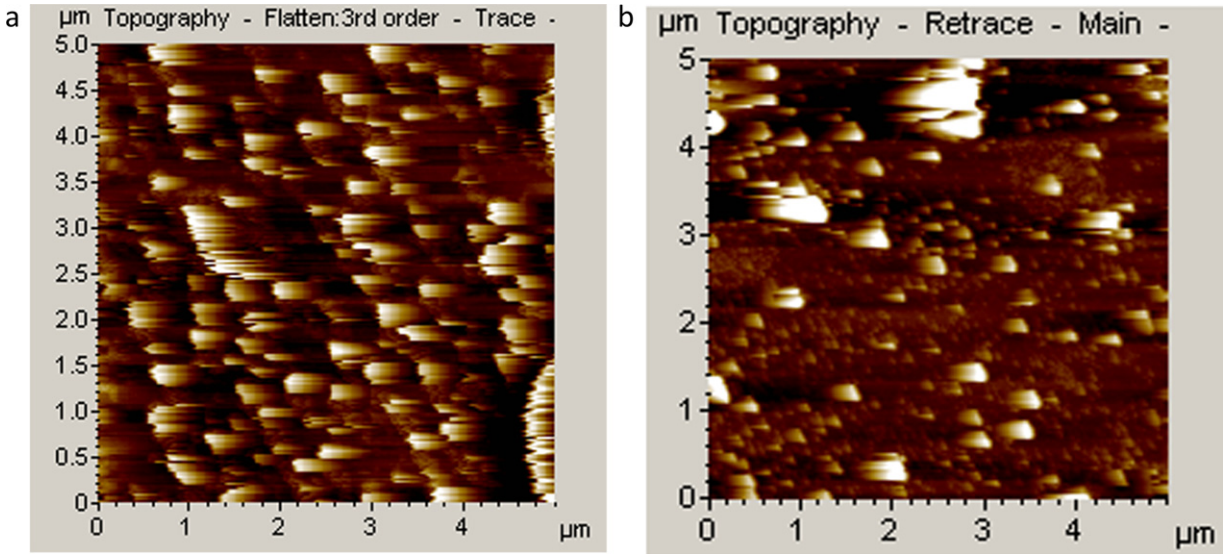

Fig. 4. AFM image of (a) J11 and (b) J21.

at T_{max} also shows a huge decease for J11, thus indicating higher thermal stability of J11.

3.6. Effect of time on acid hydrolysis

Acid hydrolysis time of sample BJ with 27 ml of 27.7% H_2SO_4 has been increased from 1 h (J11) to 2 h (J21) and 4 h (J41). The FTIR spectra for J21 and J41 are almost similar to that of J11, except that in the case of J41, the broad shoulder at 3336 cm^{-1} is almost disappeared (Fig. 1a). It is clear from the XRD data (Table 3), % crystallinity and crystallite size do not change even on increasing the time of acid hydrolysis. It is interesting to note that there is a drastic change in the morphology of the cellulose crystals, when the time of acid hydrolysis is increased (Fig. 3b–e). After 2 h of acid hydrolysis, there is a characteristic change in morphology from rod like structure (J11, Fig. 3c) to triangular shape structure (J21, Fig. 3d) with 400 nm length and 200 nm width. Further increase in acid hydrolysis time to 4 h (J41, Fig. 3e), no change in the morphology is observed, but there is an increase in size of cellulose nanowhiskers. However, the triangular shape with 500 ± 100 nm length and 150 ± 50 nm width is observed after the reduction of hydrolysis time from 1 h to 30 min (J0.51, Fig. 3b). TGA (Table 4) shows the decrease in onset of degradation (T_i) for J21 and J41 indicating more exposure to heat and therefore higher surface area as reported by Lu and Hsieh (2010). The rate of degradation at T_{max} for J21 and J41 is less compared to J11, suggesting the thermal stability of cellulose increases on increasing the acid hydrolysis time. After 1 h of acid hydrolysis, the amorphous region of the cellulose is being removed retaining the crystalline domains as described in Scheme 1 generating rod like morphology. However on increasing time, the crystalline region is hydrolyzed forming triangular shaped cellulose crystal. As a result, surface area increases leading to decrease in T_i.

3.7. Effect of temperature

Acid hydrolysis of BJ with optimized concentration of H_2SO_4 (27 ml 27.7% H_2SO_4) has been carried out for 1 h at two different temperatures *viz.* 45 °C (J11) and 57 °C (J12). A comparison of the IR spectra (Fig. 1b) shows that the peak at 1359 cm^{-1} corresponding to SO_2 stretching, is present in J12, but absent in J11. Therefore, no sulphonation occurs in case of J11 (Bhatt, Gupta, & Naitani, 2008). The intensity of the peak at 1721 cm^{-1} increases for J12, indicating presence of C=O group. For J12, the absorption band at

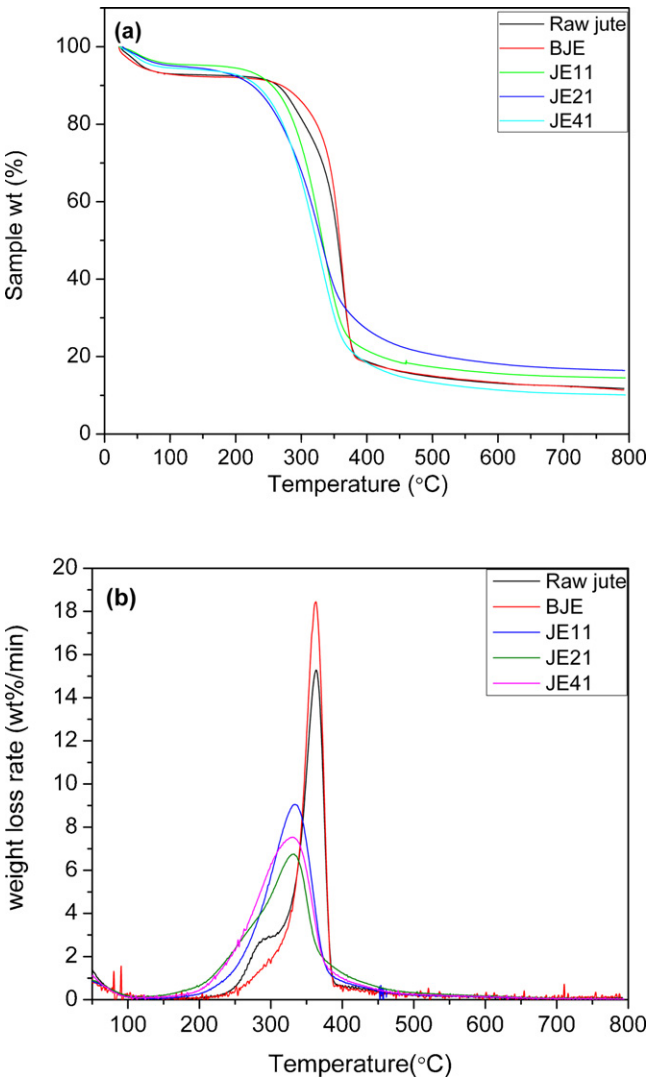

Fig. 5. Thermogravimetric curves (a) and DTG curves (b) of raw jute, BJ, J11, J21 and J41.

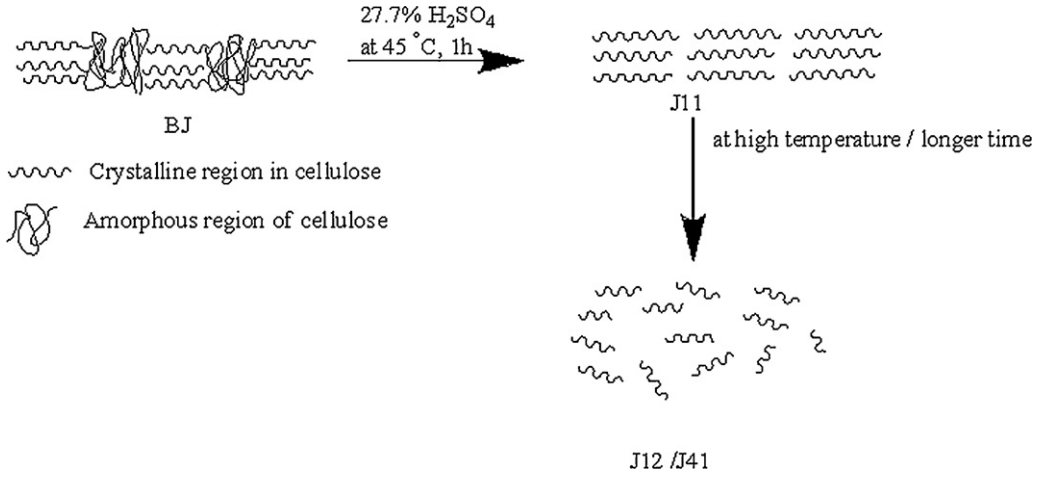

Scheme 1. Effect of temperature and time on morphology of BJ.

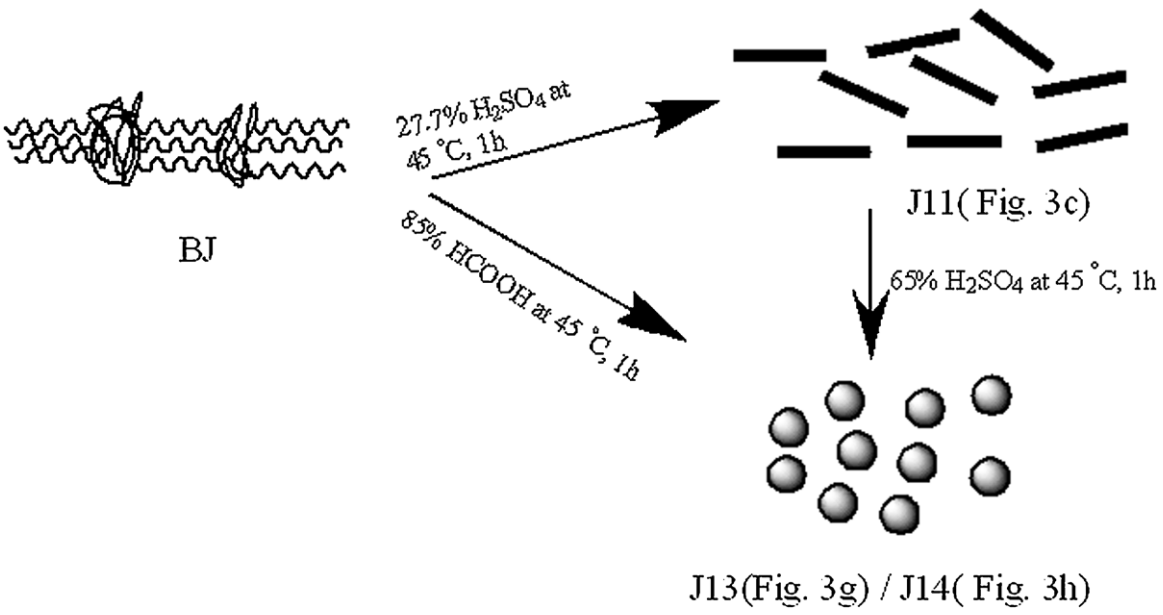

Scheme 2. Effect of different acids on morphology of BJ.

3414 cm^{-1} is almost vanished, showing absence of H-bonded O—H group (Fig. 1b). Therefore, at higher temperature, H_2SO_4 breaks the intermolecular H-bonds between the cellulose, which may lead to formation of monosaccharide (Ibrahim, Alaam, El-Haes, Jalbout, & Leon, 2006; Suganuma et al., 2008). Rod like morphology is observed for both J11 (Fig. 3c) and J12 (Fig. 3f), but the length (200 nm) for J12 is much less than that of J11. At higher temperature, the amorphous as well as crystalline region of the cellulose has been disrupted by acid hydrolysis (shown in Scheme 1) along with sulphonation.

3.8. Effect of different acids

A comparison of the formic acid hydrolysis (J13) with sulphuric acid (J11) by SEM, reveals that treatment with HCOOH leads to formation of cellulose nanoparticles as shown in Scheme 2, having diameter in the range of 46–80 nm (Fig. 3 g), whereas, rod like structure having L/D ratio – 6.5 (length – 550 ± 100 nm, width – 77 ± 30 nm) is observed for J11 (Fig. 3c), giving evidence for nanowhisker formation. Moreover, FTIR spectrum of J13 (Fig. 1b) shows a peak at 1721 cm^{-1} indicating the presence of acid (Sun et al., 2007). A broad shoulder is observed in the region of 3445 cm^{-1} giving evidence that HCOOH treatment does not break the intermolecular H-bonds (Sun et al., 2007). Therefore, treatment with HCOOH has not been found as effective pathway for cellulose whisker formation.

3.9. Effect of acid concentration

Nanowhiskers are obtained by sulphuric acid hydrolysis with an optimum low concentration (27.7%) for J11 (Fig. 3c). Cellulose nanoparticles, having diameter in the range of 46–80 nm, are observed when the concentration of sulphuric acid is higher (65%) for J14 (Fig. 3 h).

4. Conclusions

Bionanowhiskers have been successfully prepared by a simple approach based on the acid hydrolysis of jute fibers through optimization of the experimental conditions. From the above observations, the desired morphology of cellulose whiskers has been observed only for J11 after 1 h of acid hydrolysis at 45 °C. The morphology of the whiskers changes with increasing the time of acid hydrolysis as a result of disruption of glycosidic bond releasing the cellulose crystallites. In FTIR spectrum for BJ, the removal of hemicelluloses is supported by the disappearance of peak at 1738 cm^{-1} and the decrease in intensity of peak at 2921 cm^{-1}. Crystallinity of the nanowhiskers shows improvement. On increasing the concentration of H_2SO_4 from 27.7% to 65%, cellulose nanoparticles are obtained. When the temperature of the acid hydrolysis is raised from 45 °C to 57 °C, rod like morphology is found, but L/D ratio is much lower than that obtained at 45 °C. Use of formic acid instead of sulphuric acid has not been found to be useful. So, different factors like hydrolysis time and temperature, acid concentration and type of acid have a great influence on morphology as all these parameters affect domain structure of cellulose. Cellulose nanowhiskers with highest L/D ratio have been obtained after 1 h of acid hydrolysis at 45 °C with 27.7% H_2SO_4. These nanowhiskers are suitable for nanocomposite application.

Acknowledgements

The authors gratefully acknowledge Indo-Australian Strategic Research Fund, DST, New Delhi and the Commonwealth of Australia under the Australia-India Strategic Research fund for providing the financial support to carry out this work.

References

Azizi Samir, M. A. S., Alloin, F., Paillet, M., & Dufresne, A. (2004). Tangling effect in fibrillated cellulose reinforced nanocomposites. *Macromolecules*, *37*, 4313–4316.
Beck-Candanedo, S., Roman, M., & Gray, D. (2005). Effect of reaction conditions on the properties and behaviour of wood cellulose nanocrystal suspensions. *Biomacromolecules*, *6*, 1048–1054.
Bhatt, N., Gupta, P. K., & Naitani, S. (2008). Preparation of cellulose sulfate from α-cellulose isolated from *Lantana camara* by the direct esterification method. *Journal of Applied Polymer Science*, *108*, 2895–2901.
Bonini, C., Heux, L., Cavaille, J. Y., Lindner, P., Dewhurst, C., & Terech, P. (2002). Rod like cellulose whiskers coated with surfactant: a small-angle neutron scattering characterization. *Langmuir*, *18*, 3311–3314.
Cao, X., Chen, Y., Chang, P. R., Stumborg, M., & Huneault, M. A. (2008). Green composites reinforced with hemp nanocrystals in plasticized starch. *Journal of Applied Polymer Science*, *109*, 3804–3810.
Capadona, J. R., Shanmuganathan, K., Trittschuh, S., Seidel, S., Rowan, S. J., & Weder, C. (2009). Polymer nanocomposites with nanowhiskers isolated from microcrystalline cellulose. *Biomacromolecules*, *10*, 712–716.

Chen, P., Kim, H., Kwon, S., Yun, Y. S., & Jin, H. (2009). Regenerated bacterial cellulose/multi-walled carbon nanotubes composite fibers prepared by wet spinning. *Current Applied Physics*, *9*, 96–99.

Choudhury, A., Bhowmick, A. K., & Ong, C. (2010). Effect of different nanoparticles on thermal, mechanical properties of hydrogenated nitrile butadiene rubber nanocomposites. *Journal of Applied Polymer Science*, *116*, 1428–1441.

Favier, V., Chanzy, H., & Cavaille, J. Y. (1995). Polymer nanocomposites reinforced by cellulose whiskers. *Macromolecules*, *28*, 6365–6367.

Garcia de Rodriguez, N. L., Thielemans, W., & Dufresne, A. (2006). Sisal cellulose whiskers reinforced polyvinyl acetate nanocomposites. *Cellulose*, *13*, 261–270.

Goffin, A.-L., Raquez, J.-M., Duquesne, E., Siqueira, G., Habibi, Y., Dufresne, A., et al. (2011). From interfacial ring-opening polymerization to melt processing of cellulose nanowhisker – filled polylactide-based nanocomposites. *Biomacromolecules*, *12*, 2456–2465.

Ibrahim, M., Alaam, M., El-Haes, H., Jalbout, A. F., & Leon, A. (2006). Analysis of the structure and vibrational spectra of glucose and fructose. *Ecletica Quimica*, *31*, 15–21.

Kahil, A., Bhat, H. P. S., Ireana, A. H., & Yusra, A. F. (2011). Green composites from sustainable cellulose nanofibrils. *Carbohydrate Polymers*, *87*, 963–979.

Kaushik, A., Singh, M., & Verma, G. (2010). Green nanocomposites based on thermoplastic starch and steam exploded cellulose nanofibrils from wheat straw. *Carbohydrate Polymers*, *82*, 337–345.

Kvien, I., Tanem, B. S., & Oksman, K. (2005). Characterization of cellulose nanowhiskers and their nanocomposites by atomic force and electron microscopy. *Biomacromolecules*, *6*, 3160–3165.

Lu, P., & Hsieh, Y.-L. (2010). Preparation and properties of cellulose nanocrystals: rods, spheres and network. *Carbohydrate Polymers*, *82*, 329–336.

Lu, P., & Hsieh, Y.-L. (2012). Preparation and characterization of cellulose nanocrystals from rice straw. *Carbohydrate Polymers*, *87*, 564–573.

Marta, M.-Z., Amparo, L.-R., & Jose, M. L. (2011). Optimization of the nanofabrication by acid hydrolysis of bacterial cellulose nanowhiskers. *Carbohydrate Polymers*, *85*, 228–236.

Mondal, T., & Bhowmick, A. K. (2012). 2-Methyl oxazoline-grafted carbon nanofibers: preparation characterization and their role in elastomeric actuators. *Journal of Materials Science*, *47*, 4178–4186.

Oksman, K., Etang, J. A., Mathew, A. P., & Jonoobi, M. (2011). Cellulose nanowhiskers separated from a bio-residue from wood bioethanol production. *Biomass and Bioenergy*, *35*, 146–152.

Ouajai, S., & Shanks, R. A. (2005). Composition structure and thermal degradation of hemp cellulose after chemical treatments. *Polymer Degradation and Stability*, *89*, 327–335.

Pullawan, T., Wilkinson, A. N., & Eichhorn, S. J. (2010). Discrimination of matrix–fibre interactions in all-cellulose nanocomposites. *Composites Science and Technology*, *70*, 2325–2330.

Ray, D., & Sarkar, S. K. (2001). Characterization of alkali treated jute fibers for physical and mechanical properties. *Journal of Applied Polymer Science*, *80*, 1013–1020.

Rosa, M. F., Medeiros, E. S., Malmonge, J. A., Gregorski, K. S., Wood, D. F., Mattoso, L. H. C., et al. (2010). Cellulose nanowhiskers from coconut husk fibers: effect of preparation conditions on their thermal and morphological behavior. *Carbohydrate Polymers*, *81*, 83–92.

Rosa, S. M. L., Rehman, N., de Miranda, M. L. G., Nachtigall, S. M. B., & Bica, C. I. D. (2012). Chlorine-free extraction of cellulose from rice husk and whisker isolation. *Carbohydrate Polymers*, *87*, 1131–1138.

Satyamurthy, P., Jain, P., Balasubramanya, R. H., & Vigneshwaran, N. (2011). Preparation and characterization of cellulose nanowhiskers from cotton fibres by controlled microbial hydrolysis. *Carbohydrate Polymers*, *83*, 122–129.

Siqueira, G., Bras, J., & Dufresne, A. (2009). Cellulose whiskers versus microfibrils: influence of the nature of the nanoparticle and its surface functionalization on the thermal and mechanical properties of nanocomposites. *Biomacromolecules*, *10*, 425–432.

Siqueira, G., Bras, J., & Dufresne, A. (2010). Cellulosie bionanocomposites: a review of preparation properties and applications. *Polymers*, *2*, 728–765.

Suganuma, S., Nakajima, K., Kitano, M., Yamaguchi, D., Kato, H., Hayashi, S., et al. (2008). Hydrolysis of cellulose by amorphous carbon bearing SO_3H, COOH and OH groups. *Journal of the American Chemical Society*, *130*, 12787–12793.

Sugiyama, J., Chanzi, H., & Revol, J. F. (1994). On the polarity of cellulose in the cell wall of valonia. *Planta*, *193*, 260–265.

Sun, Y., Lin, L., Pang, C., Deng, H., Peng, H., Li, J., et al. (2007). Hydrolysis of cotton fiber cellulose in formic acid. *Energy & Fuels*, *21*, 2386–2389.

Terinte, N., Ibbett, R., & Schuster, K. C. (2011). Overview on native cellulose and microcrystalline cellulose I structure studied by X-ray diffraction (WAXD): comparison between measurement techniques. *Lenzinger Berichte*, *89*, 118–131.

Wada, M., Heux, l., & Sugiyama, J. (2004). Polymorphism of cellulose I family: reinvestigation of cellulose IV_I. *Biomacromolecules*, *5*, 1385–1391.